

ABSTRACT

Title of Dissertation: EVOLUTION OF PATTERNED GALLIUM
ARSENIDE (001) SURFACE SUBJECTED TO
MOLECULAR BEAM EPITAXY GROWTH

Sonam Shantilal Shah, Master of Science, 2004

Dissertation directed by: Professor Raymond J. Phaneuf
Department of Material Science and Engineering

We describe here a study of lateral length scale dependence of the transient evolution of surface corrugation during MBE growth of alternating layers of AlAs and GaAs with individual layer thickness of 50 nm (approximate configuration as used in the distributed Bragg reflectors of a VCSEL) or GaAs layers onto the patterned GaAs (001) substrates. By patterning the surface with arrays of cylindrical pits of varying diameter and spacing, we were able to study selectively the changes which occur as a function of lateral period over a range of corrugation amplitudes. The evolution in the surface morphology after various stages of growth was characterized in air with AFM.

We show that there exists a critical length scale which separates regimes of amplification and decay of corrugation amplitude with further growth. We compare our observations with the predictions of existing continuum models.

EVOLUTION OF PATTERNED GALLIUM
ARSENIDE (001) SURFACE SUBJECTED TO
MOLECULAR BEAM EPITAXY GROWTH

by

Sonam Shantilal Shah

Thesis submitted to the Faculty of the Graduate School of the
University of Maryland, College Park in partial fulfillment
of the requirements for the degree of
Master of Science
2004

Advisory Committee:

Professor Raymond J. Phaneuf, Chair
Professor Lourdes G. Salamanca-Riba
Professor Luz Martinez-Miranda

© Copyright by
Sonam Shantilal Shah
2004

Dedicated to My Parents!

ACKNOWLEDGEMENTS

I would first like to say a great big thank you to Prof. Raymond Phaneuf, for showing his extreme patience with me in completing this thesis. I would also like to thank Dr. Hung-Chih Kan, whose valuable guidance helped me out with all my problems. Three cheers to Prof. Phaneuf and Dr. Kan!!!

I am grateful to Ms. Bernadette Preston and Dr. Bill Vanderlinde for supporting me at the LPS and giving me the opportunity to use its excellent facilities.

I really appreciate the timely help I had from Taesoon, Tabassom, Tabby, Gunwoo, Dr. Tim Corrigan, Kris, Koranan, Dr. Michael Dreyer and Mark in my experiments and in general while working in the lab. You guys are the best! Thank you, Lynn Calhoun, for helping with my MBE growths.

Other people to whom I am indebted for being very valuable to me with my life and work are Vaishali, Sanjot, Jitish, Nilesh, Milind, Akanksha, my brother Siddharth, my family back home and my dear roommates.

Thank you every one for being so kind and helpful to me.

TABLE OF CONTENTS

1	Introduction	1
2	Surface Growth Models	5
	2.1 Kardar Parisi Zhang (KPZ) Equation	6
	2.2 Conserved Kardar Parisi Zhang Equation (CKPZ)	8
	2.3 Non Linear MBE equation	9
	2.4 Ehrlich-Schwoebel instability Model (ESI)	10
3	Sample fabrication	13
	3.1 Fabrication Steps	13
	3.2 Details on the Lithography Process	15
4	Experiment	21
5	Observation and Results	24
6	Summary and Future work	42

Chapter 1

INTRODUCTION

A subject of continued interest is the study of the evolution of crystalline surfaces and interfaces during epitaxial growth. The surfaces of the grown films provide an interesting testing ground for a wide range of theories and ideas related to growth dynamics. Furthermore, A variety of important semiconductor devices, such as vertical cavity surface emitting lasers (VCSEL), are composed of multi-layer thin films grown by MBE (Molecular Beam Epitaxy) and it is important to control the interfaces which separate the multiple layers of different materials in electronic and optoelectronic devices [1]. In such devices the interface roughness causes electron and/or light scattering, reducing their efficiency.

A number of groups have carried out experiments designed to understand and control the evolution of roughness of GaAs and related III-V semiconductor surfaces. Most investigations have started with a nominally flat surface, which after surface preparation contain a small degree a random uncontrolled roughness. One of the more interesting observations of an apparent instability, that of the formation of large mounded structures on a singular GaAs (001) surface was initially made by M. D. Johnson, et al., [4] and was attributed to an anisotropic sticking coefficient to ‘up’ and ‘down’ steps, a so called Ehrlich-Schwoebel barrier [2, 3]. Mound formation was also observed on growth of epitaxial GaAs (001) by other investigators [5, 6]. However, recent results from A. Ballestad, et al., [7] suggest that for homoepitaxial growth on

GaAs (001) these growth mounds in fact evolve from starting roughness on the substrate present due to desorption of the oxide at relatively high temperatures, prior to epitaxial growth.

Dependence of the rate of evolution of a corrugation on its lateral length scale is perhaps the most useful measurable quantity for comparison of experimental results with the theoretical models of growth. In standard experiments the variation of amplitude of corrugation during growth of a substrate containing some small degree of uncontrolled roughness is measured using either topographical mapping or light scattering. In this thesis I describe a more systematic approach where instead of studying evolution of random roughness we create an initial corrugation of ~ 50 nm deep, which exceeds the root mean square roughness on the unpatterned surface by more than an order of magnitude.

Patterning has been used previously by various groups, Ogino, et al., demonstrated patterning and sublimation to form ordered arrangement of bunched atomic steps on Si (111) surfaces [9]. Skutznik, et al., investigated the stability of nanostructures on Si (111) at elevated temperature [10]. Blakely, et al. used patterning and sublimation or growth to study the atomic step dynamics on periodic semiconductor surface structures [11]. Advantages of using patterning as an approach are that it allows us to study the evolution of corrugations over a range of well defined lateral length scales and over a large range of amplitudes during eventual relaxation.

We seek to describe the evolution of a patterned GaAs (001) semiconductor surface during epitaxial growth of semiconducting layers. Epitaxial growth is a process in which individual atoms or molecules are deposited from heated source cells and condense on the growing interface maintaining crystalinity. The deposited particles may stick immediately on impact, diffuse along the surface or re-evaporate from the surface. The growth is sensitive to the settings of parameters such as growth rate, system temperature, and individual component fluxes.

In the experiments described below, a GaAs (001) substrate was patterned using a photolithographic mask and then etched using reactive ion etching. The pattern is in the form an array of cylindrical pits whose diameter and center to center distance are varied in a combinatorial manner. AlAs/GaAs multi-layers and GaAs homoepitaxial layers were grown on patterned GaAs (001) substrates using MBE. Evolution in surface morphology after each growth step was characterized after transfer to atmosphere using tapping mode atomic force microscopy. The experimental results have been used to test the predictions of continuum growth models for the transient evolution of surface roughness; this regime is technologically more relevant than the asymptotic regime the models were intended to describe.

The organization of this thesis is as follows: In Chapter 2, I give a brief review of surface growth models. Chapter 3 describes of the sample preparation and the experimental apparatus. The major experimental results are presented in Chapter 4,

Chapter 5 concerns comparison to available theory and finally we summarize the results in Chapter 6.

Many of the results described here were presented in two papers both of which have been published [30, 12].

Chapter 2

Surface Growth Models

Theoretical models for surface evolution during growth can be grouped into three basic classifications; molecular dynamics models, kinetic Monte Carlo models and continuum models. Molecular dynamics models use a model potential and solve Newton's laws for each atom. Finite computational power limits the size of systems treatable to $\sim 10^4$ atoms. Kinetic Monte Carlo simulations are less deterministic, but can handle somewhat larger systems. For micron scale structures it is only feasible at present to model growth through continuum equations. Existing continuum equations for growth are based on either symmetry principles or on first principles [8, 18, and 19]. The equations have the form of a Langevin [20, 21, 22, 23, and 24] equation. In the usual approach the time dependence of the local height is written as an expansion in the height gradient and higher order spatial derivatives. As typically only a finite number of terms are included, the results have limited precision. Typically those terms thought to be important for the long term behavior, or asymptotic behavior are retained and others dropped, allowing in some cases determination of critical exponents describing growth under the assumption that scaling applies. More generally:

$$\frac{\partial h(x,t)}{\partial t} = G(h, x, t) + \eta(x, t) \quad (2.1)$$

Here $h = h(x, t)$ is the single valued interface height distribution, $G(x, h, t)$ is a general function that depends on the interface height, position and time and $\eta(x, t)$ represents random fluctuations in deposition process. The noise is often taken to have a Gaussian distribution:

$$\langle \eta(x, t) \rangle = 0 \quad (2.2a)$$

$$\langle \eta(x, t) \eta(x', t') \rangle = 2D \delta(x - x') \delta(t - t') \quad (2.2b)$$

D is a measure of the square of the noise amplitude. This expression represents uncorrelated random noise, which has a zero configuration average (random noise during deposition).

2.1 Kardar Parisi Zhang (KPZ) Equation

One of the better known continuum equations for growth was first published by Kardar, Parisi and Zhang (KPZ) [17]. In this model they suggested that growth might occur locally normal to the interface, generating a change in height δh , along the h -axis (Figure 2-1). The δh can be calculated by applying the Pythagoras theorem.

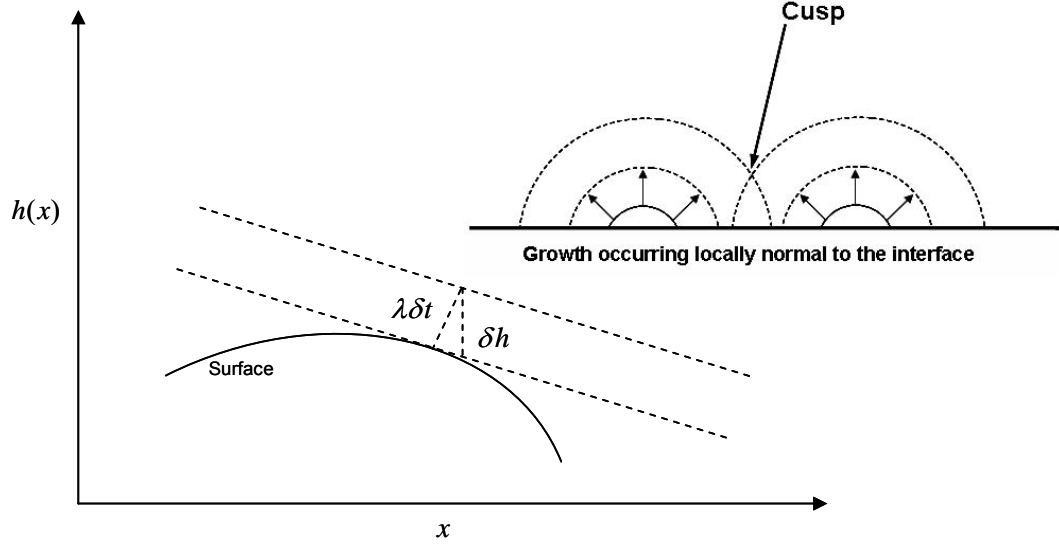


Figure 2-1: Slope dependent origin of non-linear term of KPZ model predicting cusp formation in the presence of perturbations to a flat surface.

$$\delta h = \left[(\lambda \delta t)^2 + (\lambda \delta t \nabla h)^2 \right]^{\frac{1}{2}} = \lambda \delta t \left[1 + (\nabla h)^2 \right]^{\frac{1}{2}}, \quad (2.3)$$

where λ represents the growth velocity normal to the surface.

If $|\nabla h| \ll 1$ we can expand the above equation as

$$\frac{\partial h(x,t)}{\partial t} = \lambda + \frac{\lambda}{2} (\nabla h)^2 + \dots \quad (2.4)$$

The steady interface growth λ can be excluded by a Gallilean transformation. KPZ added to this expression a surface relaxation term and random deposition noise term to write [17],

$$\frac{\partial h(x,t)}{\partial t} = v \nabla^2 h + \frac{\lambda}{2} (\nabla h)^2 + \eta(x,t) \quad (\text{KPZ equation}) \quad (2.5)$$

Here the first term is the “smoothing” term; its functional form physically corresponds to evaporation and re-condensation [37]. Its geometrical interpretation being redistribution of the irregularities on the interface, while maintaining the average height unchanged and acts as a conservative relaxation mechanism.

The second term in the KPZ equation is non-linear. It breaks the inversion symmetry of the interface height $h(x, t)$, and excess mass is being created on sloped parts of the surface. The source of the symmetry breaking is the existence of the driving force F perpendicular to the interface, which selects a particular growth direction of the interface. Objections to the KPZ equation are that it neglects the increase in growth rate with step density and that it does not obey mass conservation in a reference frame which translates upwards at a rate equal to the incident flux.

2.2 Conserved Kardar Parisi Zhang Equation (CKPZ)

A mathematically generalized mass conserving form of the KPZ equation was proposed by Sun *et al* [29], referred to here as the CKPZ model. The conserved KPZ equation is given by

$$\frac{\partial h(x, t)}{\partial t} = -\nabla^2 \left[v \nabla^2 h + \frac{\lambda}{2} (\nabla h)^2 \right] + \eta(x, t), \quad \text{CKPZ equation} \quad (2.6)$$

Where $h(x, t)$ is assumed to be a single valued function of position x and describes the height of the interface from some reference plane $h = 0$. The first term describes the dynamics of an interface involving surface diffusion with the diffusion constant proportional to v . The physical significance of the nonlinear term is unclear in this

model however. The $\eta(x,t)$ term is the noise associated with incident flux and has Gaussian distribution. The conservation of the total height is evident since the right hand side of equation (2.6) can be written as divergence of a current, and thus this has the form of a continuity equation.

2.3 Non Linear MBE equation

A nonlinear differential equation for MBE growth at intermediate to high temperatures, distinct from the KPZ equation was proposed by Lai and Das Sarma (LDS) [27] which used geometrical interpretation to study the possible linear and non linear terms in the various models of stochastically driven growing surfaces.

LDS take the surface height to be single valued in x , and expand the time dependence of height $h(x,t)$ in its local derivatives,

$$\frac{\partial h(x,t)}{\partial t} = \left(v \nabla^2 h - v_1 \nabla^4 h + \lambda (\nabla h)^2 + \lambda_1 \nabla^2 (\nabla h)^2 + \lambda_2 \nabla (\nabla h)^3 + \dots \right) + \eta(x,t) \quad (2.7)$$

They then argue that the first and the third term on the right hand side of the equation should be neglected since in MBE the energy scale is set by atomistic scale bonding and at the usual MBE growth temperatures desorption is an exponentially weak process. They also argue that so far, no physical mechanism generating the λ_2 term has been discovered and it is assumed to be a higher order correction of the $\nabla^2 h$ relaxation process, hence it is neglected. The strong chemical bonding situation of MBE is the physical interpretation for the v_1 term, where the atoms can stick to kink

sites rather than rolling down to the local height minima. They argue that a ‘positive’ λ_1 term (which is negative in case of conserved KPZ equation) would correspond to the high temperature regime where surface atoms at the kink sites can break bonds and hop with larger probability to steps with smaller heights. This reduces the equation (2.7),

$$\frac{\partial h(x,t)}{\partial t} = -v_1 \nabla^4 h + \lambda_1 \nabla^2 (\nabla h)^2 + \eta(x,t) \quad (\text{LDS Model}) \quad (2.8)$$

2.4 Ehrlich-Schwoebel instability Model (ESI)

A model based on microscopic physics suggesting an explanation for “mound” formation during homoepitaxial growth on nominally flat GaAs (001) surface due to the so-called “Ehrlich-Schwoebel effect” was proposed by Johnson *et. al.* [28]. The additional barrier for an adatom to hop across a surface step in the descending direction is known as the Ehrlich-Schwoebel barrier (referred here as S_c). Physically it corresponds to the need for a diffusing atom to essentially break a set of bonds before a new set can begin to form on crossing the step edge.

In this model a surface current,

$$\hat{j} = FS_c \sigma^2 \frac{\nabla h}{1 + (\sigma m)^2}, \quad (2.9)$$

which peaks at slope $m = |\nabla h| = \frac{1}{\alpha\sigma}$, (where α is a constant of order unity) was proposed. Here F is the incident particle flux, S_c is a factor deriving from the Schwoebel barrier, σ is the diffusion length on a terrace. The diffusion length σ , is the average distance an atom will travel before it collides with other atoms to form an island on the surface. The uphill current for small slopes will be limited by this diffusion length. For large slopes the limitation is due to decreased length of the terrace and diffusion of the edge atoms over the Schwoebel barrier. This process becomes more likely as steps get closer. The growth equation is of the form

$$\frac{\partial h(x,t)}{\partial t} = -\nabla \cdot \hat{j} + \eta(x,t) \quad (2.10)$$

where \hat{j} is a function of the local slope. From (2.9), in the limit of small slope the current j is proportional to $|\nabla h|$, while in the limit of large slope the current \hat{j} is proportional to $\frac{1}{|\nabla h|}$.

To compare the prediction of the continuum models described above with our experimental results, we first measure the topography of the patterned GaAs (001) surface without any growth and use this to set the initial conditions for our numerical simulations. The continuum equations are integrated using the finite difference method [12, 34, and 35]. The anisotropy that we see in our results (discussed in detail in the subsequent chapters) between the [1 1 0] and [1 -1 0] directions, is introduced using the anisotropic version of the above continuum models [27, 28, 29, 34, and 17].

The results of the numerical simulations and its comparison with our experimental results are explained in detail in Chapter 5.

Chapter 3

SAMPLE FABRICATION

For the experiments conducted in this work we chose to fabricate periodic arrays of cylindrical pits on the surface of the sample (Fig 3-1). These periodic arrays of cylindrical pits were made on semi-insulating (SI) (001)-oriented, gallium arsenide (GaAs) by standard photolithography processing in conjunction with a dry reactive ion etching system. The GaAs wafers used were supplied by American Xtal Technology [16]. The fabrication requires several steps and exposure to several solvents. The process is illustrated schematically in Fig 3-2. A detailed process description follows. All fabrication was performed in a Class 10 cleanroom to minimize contamination by particulates. The cleanliness of the sample is crucial as the experiments involve regrowth using the molecular beam epitaxy (MBE) process which is sensitive to surface contamination.

3.1 Fabrication Steps

The GaAs (001) wafers used in these experiments were two inches in diameter and 500 +/- 25 μm thick. The surface orientation was (001) to within +/- 0.5°. To transfer the pattern to the wafer we used a standard lithography process, using specially designed masks and a GCA 200 ALS 5:1 stepper with nominal resolution of 0.5 micron. Exposure, developing and liftoff was followed by reactive ion etching. A Negative mask was used for the experiments since we found it easier to eliminate residual photoresist after transferring of the pattern to the GaAs substrate using a

negative photoresist (NR7-1500 from the Futurrex Inc. [13], later a new recipe using a positive photoresist where it's even easier to remove the residual photoresist was found out. But the samples used in this thesis were made using negative photoresist). After the lithography process $\sim 50\text{nm}$ deep cylindrical pits are dry etched by reactive ion etching. The remaining resist was then removed by dissolving it in solvents. The details of the above processes are explained in the following sections. The sample was then installed into the MBE chamber for growth.

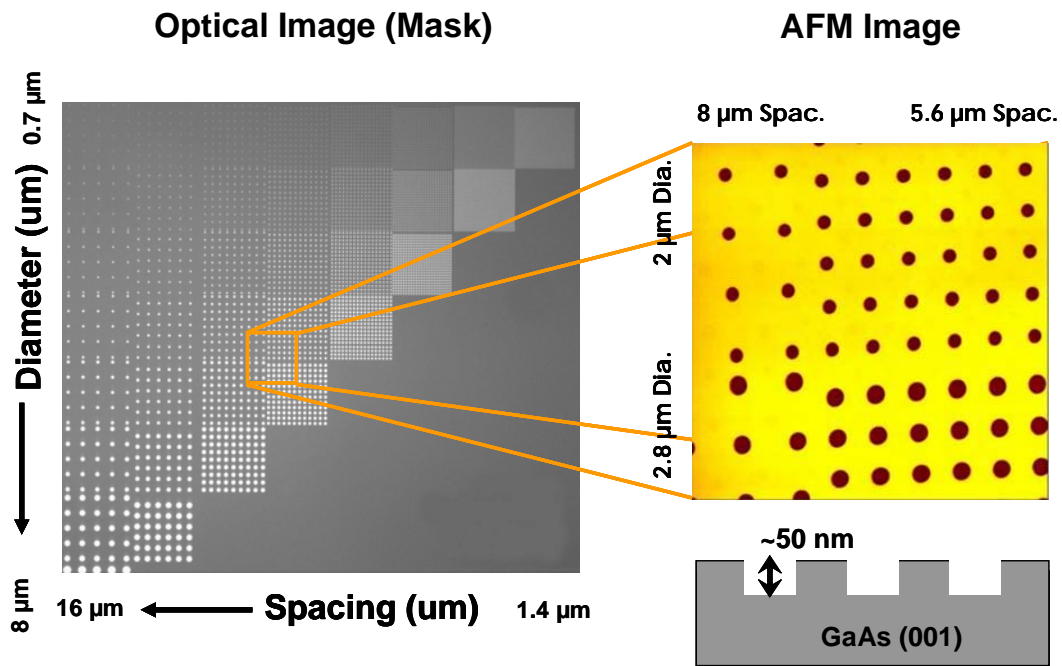


Figure 3-1 Optical image of the mask used in preparation of the patterned GaAs (001) surface. The spacing between the cylindrical pits and its diameter varies across the horizontal (16 micron – 1.4 micron) and vertical direction (0.7 micron – 8 micron) respectively. The spacing between pits is twice the pit diameter along the diagonal cells. The initial depth of corrugation is $\sim 50\text{ nm}$ which is same as the thickness of the individual distributed bragg reflector layer.

3.2 Details on the Lithography Process

The overall process is shown schematically in (Fig 3-2). GaAs (001) wafer obtained from the manufacturer is first cleaned using Trichloroethylene (TCE), Acetone, Methanol and Isopropyl Alcohol (IPA) solvents in a standard laboratory ultrasonic cleaner followed by rinsing in flowing Deionized (DI) water and dried by blowing dry nitrogen gas. I followed the procedures developed by my predecessor in the group, Koranan Limpaphayom [31]. Table 3-1 below shows the time and order in which the solvents were used.

<i>Solvents</i>	<i>Time</i>
<i>Trichloroethylene (TCP)</i>	3 minutes in ultrasonic cleaner
<i>Acetone</i>	3 minutes in ultrasonic cleaner
<i>Methanol</i>	3 minutes in ultrasonic cleaner
<i>Isopropyl Alcohol (IPA)</i>	3 minutes in ultrasonic cleaner
<i>Deionized Water</i>	3 Minutes flowing water

Table 3-1: Solvents used for cleaning the wafer

After cleaning the wafer ~ 1000 °A of SiO₂ was deposited on the wafer using a Plasma Enhanced Chemical Vapor Deposition system from Plasmalab [14] using parameters listed in Table 3-2. The deposited SiO₂ layer acted as a sacrificial layer, and prevented direct contact of resist with the GaAs surface.

<i>Deposition Rate</i>	~165 A/min
<i>N₂O Gas</i>	12 sccm (put in number 60%)
<i>2% SiH₄ / N₂ Gas</i>	64 sccm (put in number 32%)
<i>Total Chamber Pressure</i>	300 mTorr
<i>Substrate Temperature</i>	0 (300 °C at temp. controller)
<i>RF Power</i>	10 W (4.4%)
<i>Time</i>	6 minutes

Table 3-2: Parameters for depositing SiO₂ layer on the GaAs (001) substrate with Plasma Enhanced Chemical Vapor Deposition system [31, 32]

Hexamethyldisilazane (HMDS), which acts as an adhesion promoter of the photoresist to the wafer was spun at 2000 rpm for 60 seconds. Several drops of NR7-1500 negative photoresist was then put on the wafer with a disposable pipette and immediately spun at 5000 rpm for one minute. The spin created a uniform thickness of ~one micron. The sample was then put on a hotplate and prebaked at 120 °C for 60 sec to harden the photoresist and make it adhere to the sample surface. The sample was then transferred to the stepper to do exposure. The operating parameters, finalized by a trial and error process are summarized in table 3-3. [31, 32]

<i>Focus</i>	9
<i>Wavelength</i>	365 nm
<i>Exposure time</i>	9.25 sec

Table 3-3: Parameters for photolithography in the stepper system.

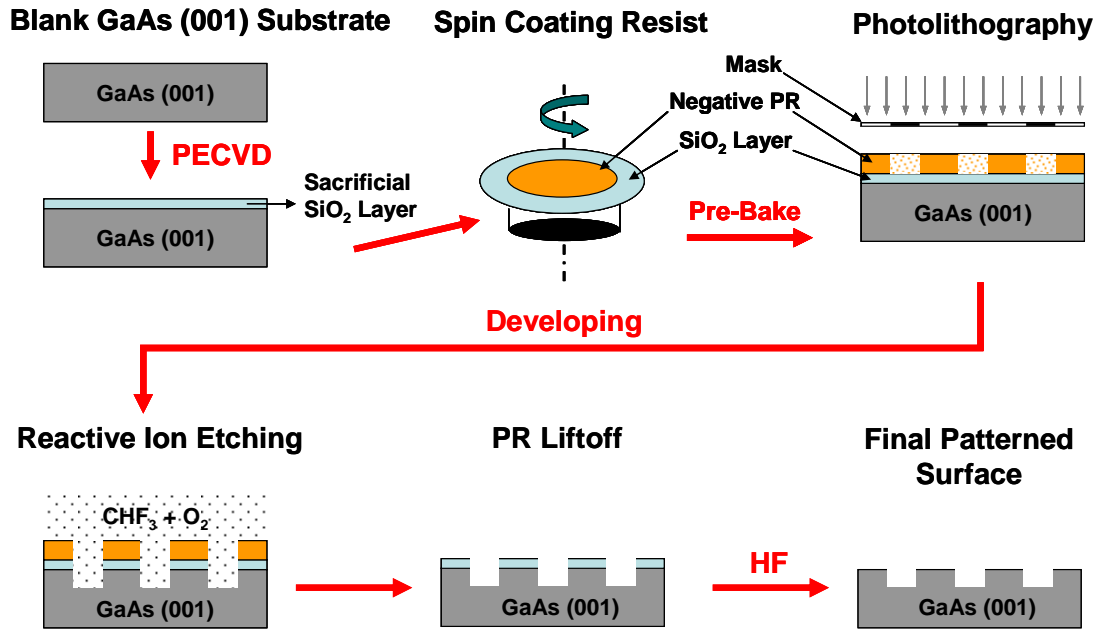


Figure 3-2: Schematic diagram of the process used in preparation of the patterned GaAs (001) substrates used in our experiments.

Once exposure was done samples were postbaked at 120 °C for 60 sec to harden the negative photoresist so that the exposed pattern was retained. After postbake the exposed photoresist on the sample was developed with the resist developer (RD6 from Futurrex Inc) for 10 seconds. The sample was then rinsed in flowing Deionized (DI) water for approximately one minute and finally dried with dry nitrogen gas.

The pattern was then transferred to the each sample with developed photoresist using the reactive ion etching system. Our final etched depth is ~50 nm. This depth is same as the thickness of the individual layers of the distributed bragg reflectors of the VCSEL device. To have more control over the anisotropic etching process dry etching using the reactive ion etching system (Plasmatherm RIE Model 790) was used. The operating parameters for the process used are given in table 3-4.

<i>ChF3 Gas</i>	80 %
<i>O2 Gas</i>	20 %
<i>RF power</i>	175 W
<i>Pressure</i>	40 mTorr
<i>Time</i>	12 minutes

Table 3-4: Parameters for dry etching in the Plasmatherm reactive ion etching system [31, 32]

After the pattern was transferred to the sample the remaining resist was removed using resist remover RR2 from Futurrex Inc, at 110 °C for 15 minutes followed by deionized (DI) water rinse for approximately one minute. The wafer was then cleaned with acetone, methanol, and isopropyl alcohol (IPA) solvents for one minute each and dried using nitrogen gas. The SiO₂ sacrificial layer was then removed by dipping it in a buffered oxide etch Solution (HF) (10:1) for 20 sec followed by DI rinse for two minutes and N₂ Dry. The residual photoresist from the surface after the standard liftoff process using RR2 did not completely remove all of the photoresist residues (Fig 3-3 (a)). We therefore etched the wafer in an oxygen plasma asher system (Matrix System One Stripper Model 102) for one minute. Then the sample was immersed in 1-Methyl-2-Pyrrolidinone (NMP) solution at 80C for 30 minutes followed by rinsing it in trichloroethylene, acetone, methanol, isopropyl alcohol, DI water and Isopropyl Alcohol for 1 minute each and N₂ dry. These last two steps, using the plasma asher and NMP were repeated until we had a clean surface on the sample without any residue, as judged by imaging with atomic force microscopy (Fig 3-3 (b)).

<i>Pressure</i>	5.00 Torr
<i>MFC 1</i>	55 %
<i>MFC 2</i>	0 %
<i>MFC 3</i>	0 %
<i>RF FWD</i>	500 Watts
<i>EP Mode</i>	(0) Timed = 3 min. 0 seconds
<i>Filter</i>	2

Table 3-5: Parameters for the ‘Strip’ process used in the Matrix System One Stripper Model 102 system [31, 32].

Once the patterned sample was cleaned, initial measurements of the surface morphology before growth were made in ‘tapping mode’, in air, using an atomic force microscope (Digital Instruments DI Model 3100) [15]. Typically two complete super-cells were imaged from different regions on the wafer to allow uniformity of etching to be judged. The samples were next loaded into the molecular beam epitaxy (MBE) machine (EPI, model 1040) [15].

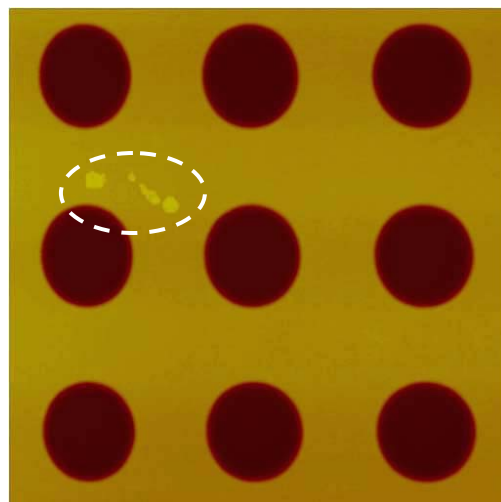


Figure 3-3 (a): AFM image of the patterned GaAs (001) surface after liftoff showing residual resist

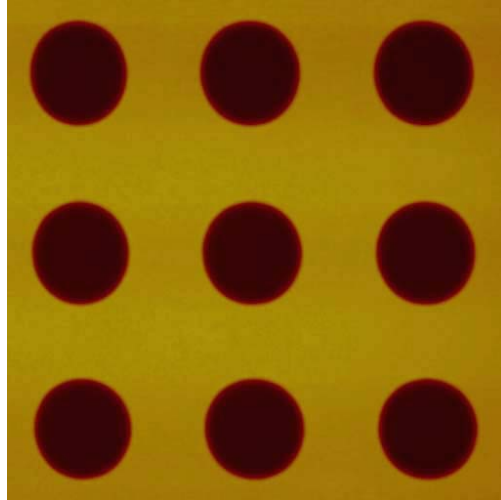


Figure 3.3 (b): AFM image of a clean patterned GaAs (001) surface after Asher/NMP cleaning

Chapter 4

EXPERIMENT

The experiments consisted of growing alternating layers of AlAs and GaAs with individual layer thickness of 50 nm or GaAs layers onto the patterned substrates. The chosen thickness of the alternating layers is same as the thickness of the individual layers of the distributed bragg reflectors of the VCSEL device. We cycled the samples between the MBE growth chamber, and the AFM. The summary of the experimental procedure is shown in Figure 4-1.

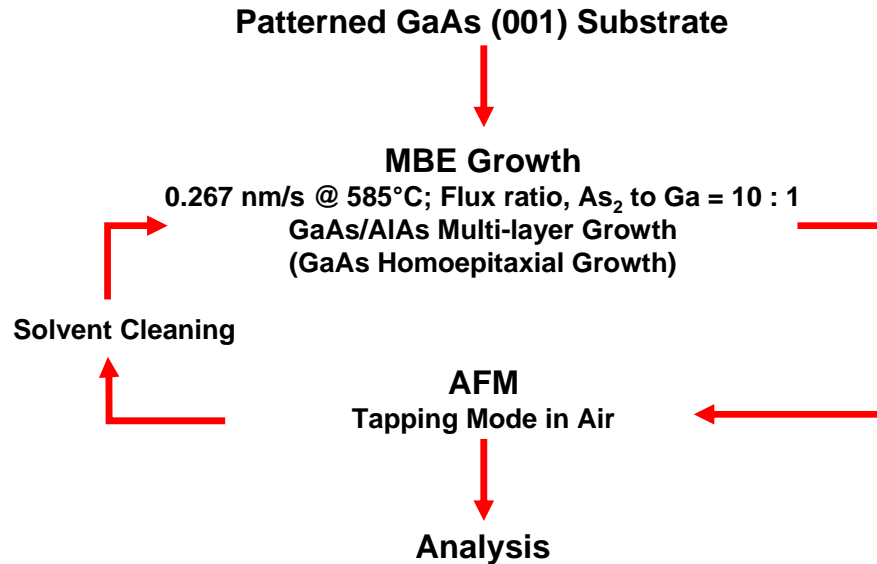


Figure 4-1: Summary of the experimental procedure.

Because of the extreme sensitivity of MBE growth to surface contamination samples were cleaned again with solvents using the procedure mentioned in Chapter 3 (Section 3.2, Table 3.1) subsequent to AFM imaging. Each sample was inspected

under intense optical light for unusual reflections which might indicate residual contamination. Samples which appeared uniform were introduced into the MBE station

Each sample was kept in the introduction chamber of the MBE system, and degassed for 12 hrs at 180 °C in a background pressure of approximately 10^{-11} torr. Next samples were transferred into the preparation chamber ($P = 10^{-11}$ torr) where the second stage of degassing of the sample, for 30 minutes at 400 °C is carried out. Prior to growth the beam equivalent pressure (BEP) of As₂, Ga and Al was measured using an ion gauge in the growth chamber, while the sample was still in the second stage of degassing in the preparation chamber. The BEP for As was fixed to be 10 times that for Ga or Al [33], a fairly standard ratio for ‘flat’ MBE growth. The growth temperature of the substrate was 585 °C with a growth rate of 0.267 nm/s. After transferring to the growth chamber, the sample was heated to the growth temperature, rotated at 10 rotations per minute and desorption of the oxide was monitored using RHEED (Reflection High Energy Electron Diffraction). As the oxide is removed the RHEED pattern was observed to develop into diffraction streaks characteristic of an ordered (100) surface.

Two types of experiments were carried out, the growth of AlAs/GaAs multilayers, and the homoepitaxial growth of GaAs on patterned GaAs substrates. In the first case we chose individual layer thickness equal to 50 nm, so that a period consisted of 50 nm AlAs / 50 nm GaAs, with the final surface always GaAs. We performed growths of 1 period, 5 periods, 10 periods, and 50 periods. Similar growth procedures and

parameters were maintained for the patterned GaAs homoepitaxial growth experiments with a total thickness of 100 nm, 200 nm, 300 nm, 500 nm, and 2000 nm grown. After each growth experiment the evolution in surface morphology was characterized using tapping mode AFM in air.

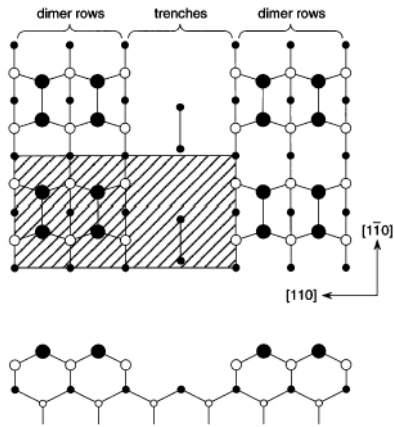
AFM images of the surface morphology after growth show that the MBE growth results in a nonmonotonic; anisotropic evolution of the patterned structures. We present these results in detail in the following chapter.

Chapter 5

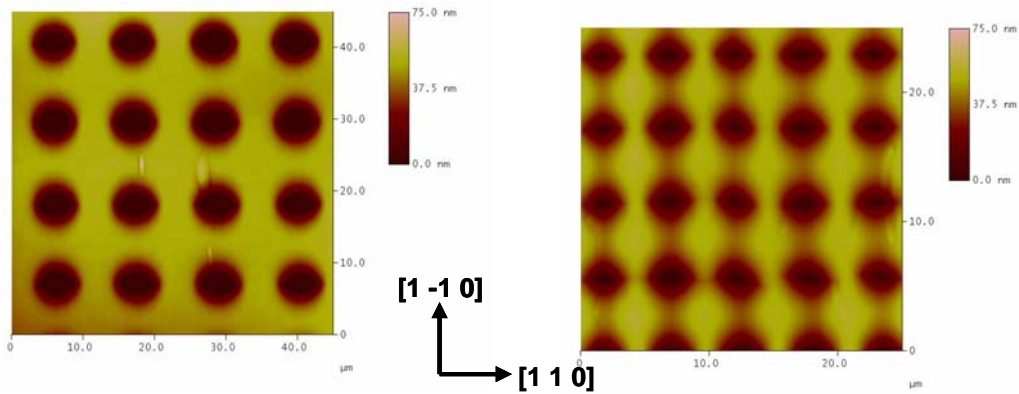
OBSERVATION AND RESULTS

Growth from the flat area of the sample, between pits, was in the mode of island nucleation and growth, as revealed from the AFM images. In this thesis we mainly focus on the results obtained from the patterned area.

AFM images of the surface morphology of the patterned GaAs (001) surface, at different length scales, after a total of 50 periods of AlAs/GaAs multi-layer growth are shown in Fig 5-1. The images are in the same data scale. They show that the growth results in an anisotropic evolution of the patterned surface structures, with each circular pit evolves faster along the $[1 -1 0]$ direction and slower along the $[1 1 0]$ direction resulting in the eccentricity in its shape. This anisotropy is related to the β_2 (2 x 4) reconstruction of the GaAs (001) surface. Itoh, et al., interpret the differences as mainly coming from an asymmetry in the Ga sticking coefficient for steps along these two directions (Fig- 5-1 (a)). [25 and 26]. The images also show a length scale dependence on the evolution. Large scale structures (for ex. Fig 5-1 (b)), shows slight blurring at the edges without any significant change in corrugation amplitude. The circular shape pits eventually becomes more elliptical in shape due to the anisotropy during growth (for ex. Fig 5-1 (c)). The pits then smear into each other along the $[1 -1 0]$ direction and it looks like a bunched column-wise structure (for e.g. Fig 5-1 (d)). There is a large decrease in the corrugation amplitude of the small scale structures (for ex. Fig. 5-1 (e)) with prominent material buildup between the original pits, giving rise to bunch ridges along $[1 -1 0]$ direction.

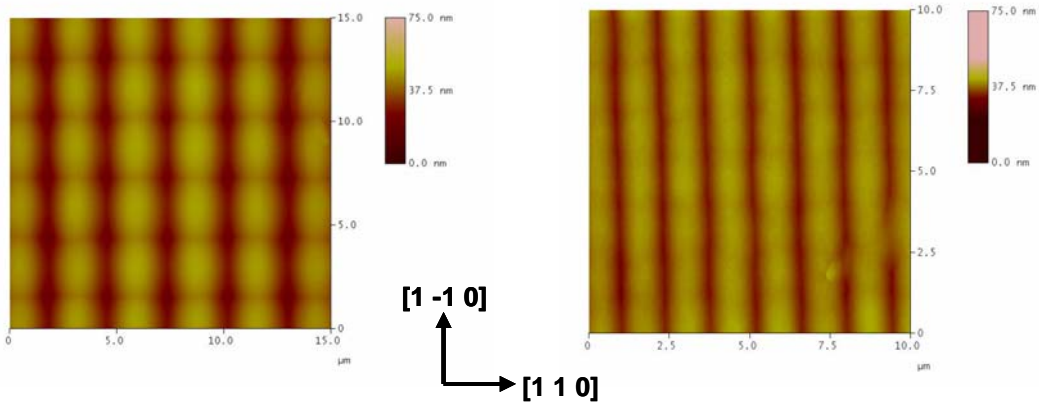


a) Side and plan views of the β_2 (2 x 4) reconstruction of GaAs (001) surface. The darkened circles represent As atoms and the open circles represent Ga atoms. The (2 x 4) surface unit cell is indicated by shading [26].



b) 5.6 μm Diameter and 11.2 μm Spacing

c) 2.8 μm Diameter and 5.6 μm Spacing



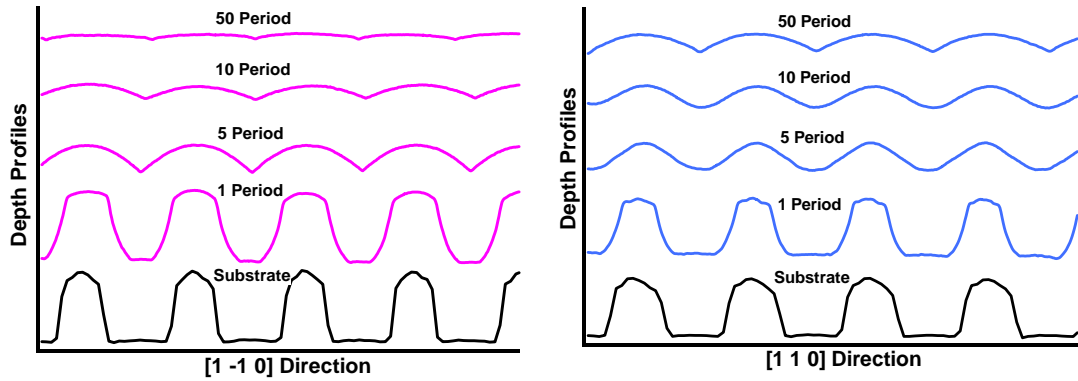
d) 1.4 μm Diameter and 2.8 μm Spacing

e) 0.7 μm Diameter and 1.4 μm Spacing

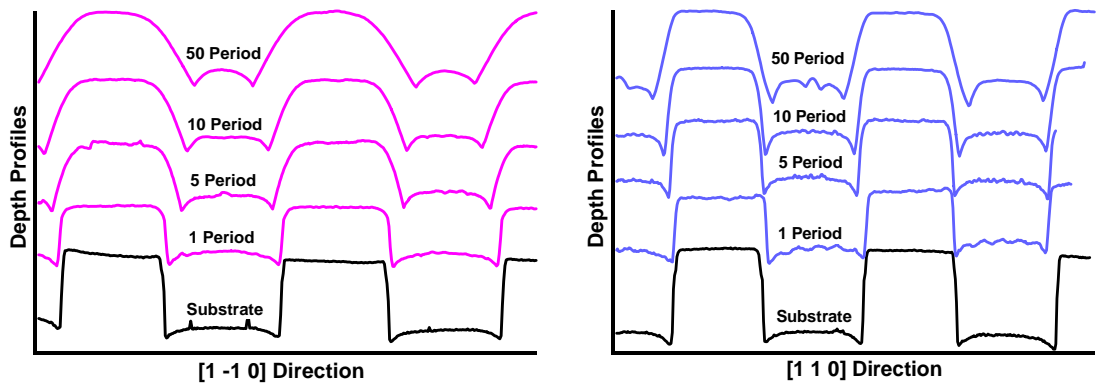
Figure 5-1 (a): β_2 (2 x 4) reconstruction of GaAs (001) surface. (b - e) Atomic Force Microscopy images of the surface morphology after a total of 50 periods of AlAs/GaAs Multi-Layer growth on the patterned GaAs (001).

Looking in detail, the typical history of evolution of a particular length scale in terms of depth profiles scanned across the pit centers along the $[1 \ -1 \ 0]$ and $[1 \ 1 \ 0]$ directions is illustrated in Figures 5-2.

Profile of the substrate (note the exaggerated depth scale) shows nearly cylindrical pits with etching induced artifacts, one being the rounding of the upper shoulders of the pits and an apparent trench around the bottom edges; this can be easily seen for the larger diameter pit arrays. Considering Figure 5-2 (a), the first period of AlAs/GaAs Multi-layer growth the sharp corners seen in the substrate profile of the pits gets rounded. With further growth, the side walls of the pit close along the $[1 \ -1 \ 0]$ direction and forms a cusp at the center of each pit, which persists with growth before smoothening out. On the other hand, the line profile along the $[1 \ 1 \ 0]$ direction first evolves into a sinusoidal modulation which only after much thicker growth forms cusps and decays eventually. The line profiles taken across the largest diameter pits (Fig 5-2 (b)) shows a slow decay as compared to the smaller diameter pits. Here too with initial growth there is rounding of sharp corners. The trenches at the bottom of the pits deepens with further growth and the evolution is faster along the $[1 \ -1 \ 0]$ direction.



a) 1.0 micron diameter and 2.0 micron spacing



b) 8.0 micron diameter and 16.0 micron spacing

Figure 5-2: Evolution of Depth profiles across pit centers along the $[1 -1 0]$, $[1 1 0]$ directions for AlAs/GaAs Multi-Layer growth on patterned GaAs (001).

The changes in the evolution of the structures during growth during the multi-layer growth are non-monotonic, both with respect to the length scale and the thickness grown. Figure 5-3 shows the summary plot of the evolution of the corrugation amplitude after the various stages of growth along the fast and slow evolution directions. The change in the corrugation amplitude is measured by measuring the depths after various stages of growth from the depth profiles (Fig 5-2) taken across the center of the pits along the two evolution directions. The errors bars shown are the standard deviation values of at least sixteen measurements taken per data point. It can

be easily interpreted from the summary plot that the changes are quite large and exceed the uncertainty given by the error bars. After the first period of growth, the corrugation at the smallest period increased slightly from its initial value of 50 nm. With further growth the length scale dependence shows a characteristic peak; the diameter corresponding to the maximum in each plot divides the trend in evolution. For the pits with initial diameter smaller than this, further growth reduces the corrugation amplitude and the pits with diameter greater than this further growth amplifies the corrugation. The peak shifts to larger diameters with further growth signifying that eventually even larger length scale structures relax.

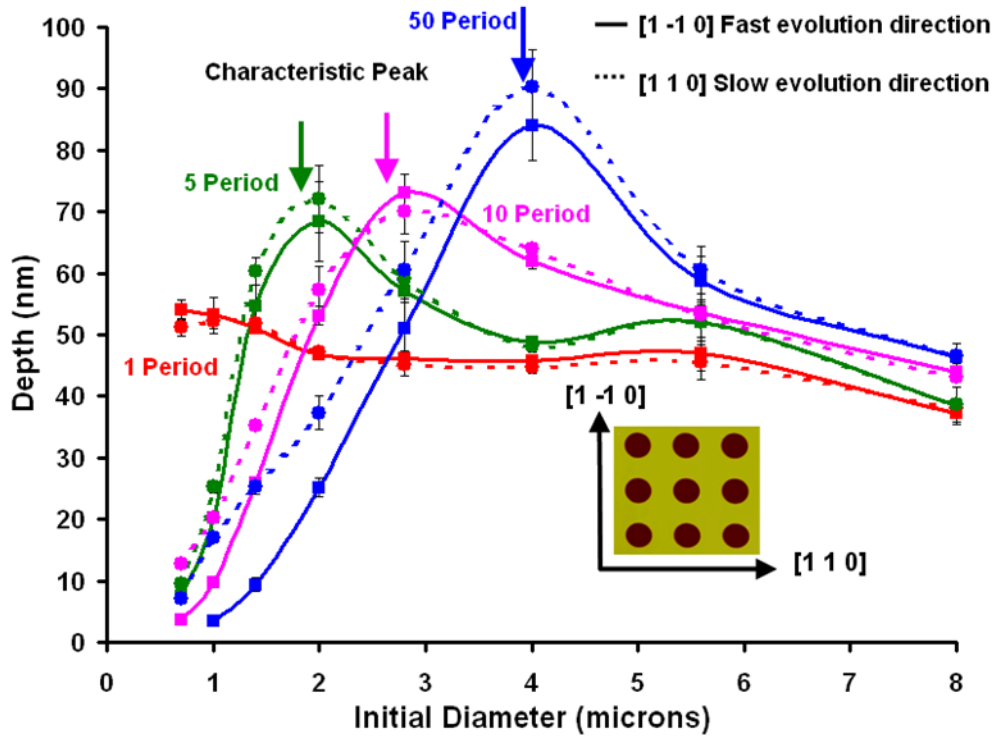
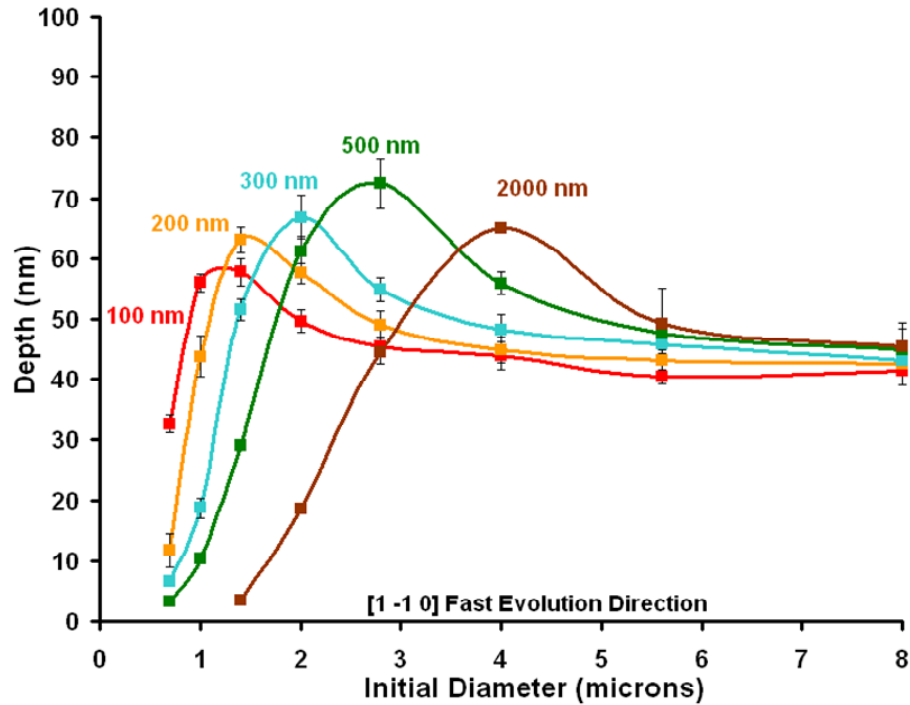
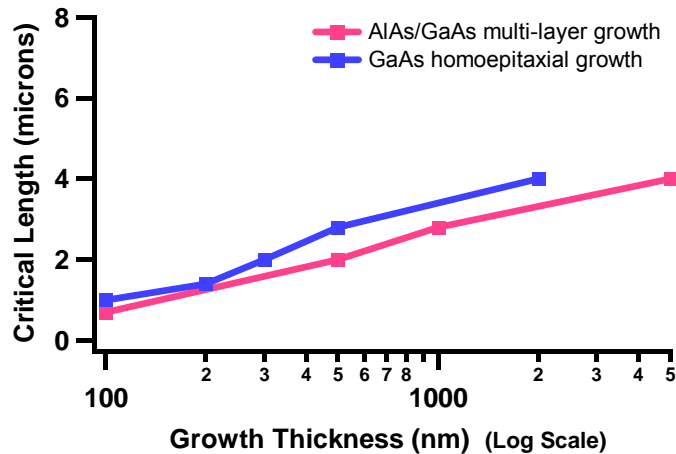


Figure 5-3: Summary plot showing the length scale dependence of the evolution of the corrugation amplitude of the surface after various stages of growth along the $[1 -1 0]$ and $[1 1 0]$ directions for AlAs/GaAs multilayer growth on patterned GaAs (001). Here the distance between the center to center spacing between pits is twice the pit diameter.

There may be effects of the slight mismatch (0.14%) between the lattice constants of AlAs and GaAs on very lateral length scales. Also it is likely that the kinetic effects, such as the Schwoebel barrier will be different for Al and Ga affecting the growth. This motivated us to do control experiments, of growing GaAs on patterned GaAs (001) surfaces using the same procedures. As shown in Fig 5-4, the changes seen in the evolution of structures are non-monotonic and are qualitatively similar to those seen during the AlAs/GaAs multilayer growth. However, the peaks separating amplification from decay as a function of growth are shifted slightly to larger length scales for the same amount of growth (Fig 5-3 (b)). And this might be due to the slight lattice mismatch between the AlAs and GaAs. Thus the existence of a critical length scale which separate regimes of amplification and decay seems to be a general feature of MBE growth in the GaAs/AlAs system at this temperature, flux ratio and growth rate.



a) Length scale dependence of the evolution of the corrugation amplitude after various stages of GaAs homoepitaxial growth.



b) Position of the peak (from the summary plot, Fig 5-3 and Fig 5-4 (a)) during various stages of growth for AIAs/GaAs multilayer growth and GaAs homoepitaxial growth.

Figure 5-4: Summary plot showing the length scale dependence of the evolution of the corrugation amplitude of the surface after various stages of growth along the $[1 -1 0]$ direction for homoepitaxial growth on patterned GaAs (001). (b) Shift in the peak position for GaAs homoepitaxial growth to larger length scale for the same amount of growth.

The data analyzed in the summary plots (Fig 5-3, Fig 5-4) were calculated considering the depths from the center of the bottom of the pits where there is more variation in growth as compared to the edges of the cylindrical pits. To be sure whether these variations do not affect the results significantly we also calculated the depths from the edges of the bottom of the cylindrical pits. The resultant summary plot looks qualitatively similar indicating that choosing this as the measure of the corrugation does not affect the overall trend in evolution.

We have also examined the evolution of the corrugation amplitude of the surface after growth for constant spacing between the pits and varying pit diameters i.e. the diameter dependence shows the results are qualitatively similar showing a peak separating regimes of amplification and decay with further growth. The study of spacing (pitch) dependence shows the evolution is quite different although there is an initial regime of amplification followed by decay. The decay is fast for smaller spacing but nearly uniform beyond critical spacing (Fig 5-5) which gradually seems to move to higher values with further growth. This shows that the spacing between the pits dominates the evolution of the structures.

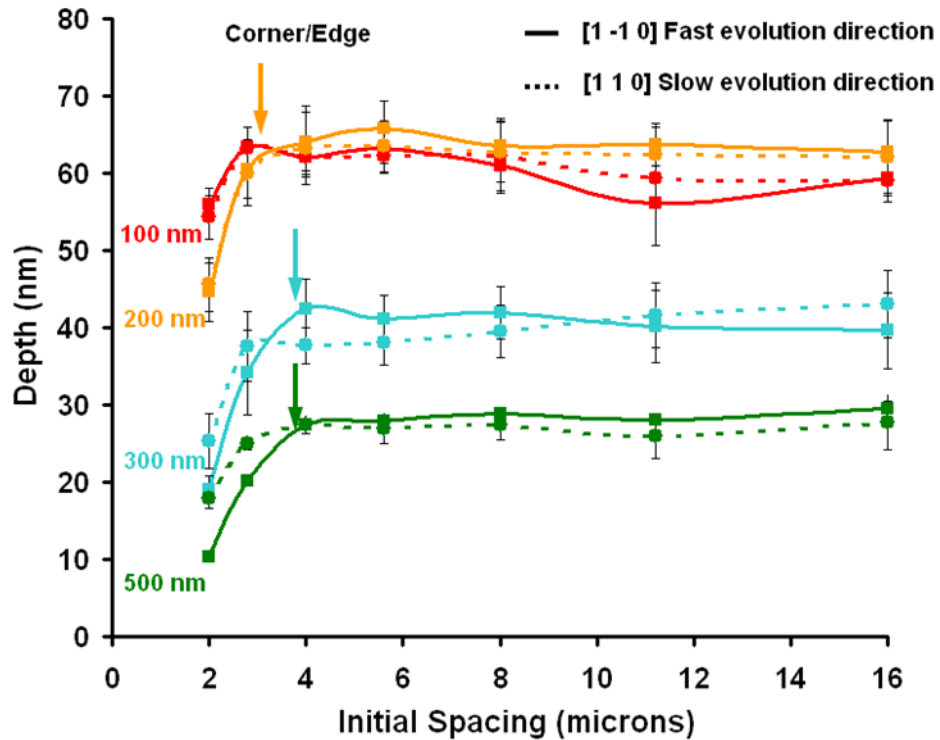
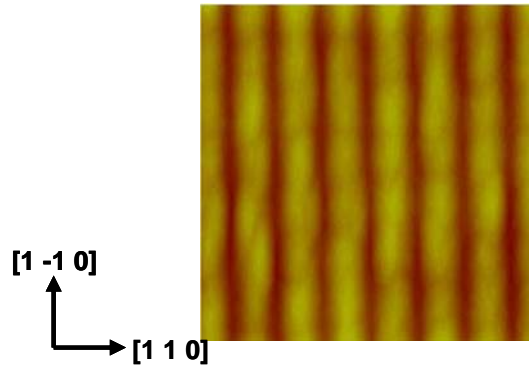


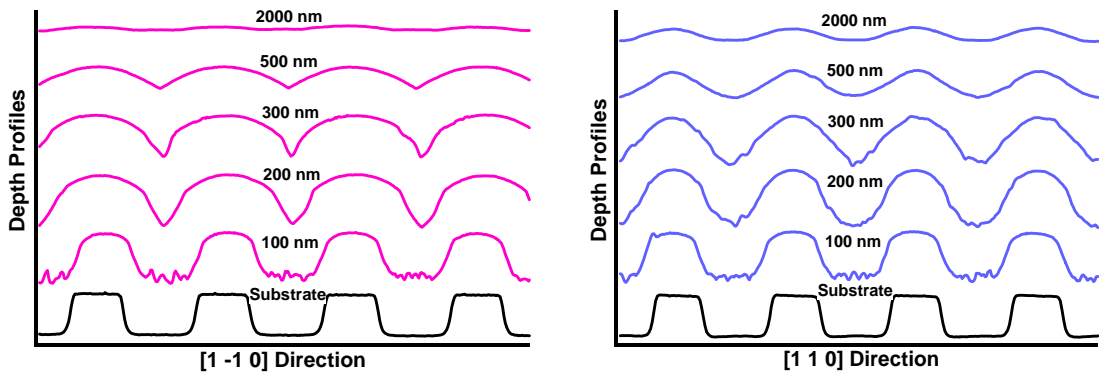
Figure 5-5: Summary plots showing the pitch dependence of the evolution of the corrugation amplitude of the surface after various stages of growth along $[1 -1 0]$ $[1 1 0]$ directions for homoepitaxial growth on patterned GaAs (001), for an initial pit diameter of 1 micron.

The thickness dependent critical pattern length scale (Fig 5-3, Fig 5-4) separating regimes of amplification and decay of corrugations with further growth means that there are at least two effects competing during growth. One acts to smooth out the perturbations, the other causes to increase the roughness of the surface with further growth. These effects and the resulting crossover from amplification to decay must be a part of any model used to describe the MBE growth in this system. Below we consider a number of continuum growth models in which competing effects occur. Most of the continuum models [9, 20, 52, 53 and 54] have been constructed to describe the asymptotic behavior of the evolution of the surface roughness for an

initially flat surface during epitaxial growth while our measurements reveal the transient response of the system. Nevertheless this latter regime is more practically relevant and thus can be used to assess the validity of these models in describing the transient evolution.



a) Surface Morphology of 0.7 micron diameter and 1.4 micron spacing region after 2000 nm growth



b) Depth profiles along the orthogonal directions

Figure 5-6: Surface Morphology and Depth profiles for homoepitaxial growth on the patterned GaAs (001). (b) Additional roughness can be seen at the bottom of the pits presumably induced by the initial roughness produced by reactive ion etching process used to pattern the substrate. This roughness does not affect our results qualitatively. Also the depth profiles are taken from a smaller scan size compared to shown in (a).

Simulations based on the four models explained in Chapter 2 were carried out for GaAs homoepitaxial growth on a region with initial pit diameter 0.7 micron and 1.4

micron spacing. Surface Morphology and Depth profiles for the same region from our experiments are shown in Fig 5-6.

The smoothing term in the height evolution equation $v \cdot \nabla^2 h$ is replaced with $v_x \cdot \frac{\partial^2 h}{\partial x^2} + v_y \cdot \frac{\partial^2 h}{\partial y^2}$, and the growth related non-linear term $\lambda \cdot (\nabla h)^2$ is replaced

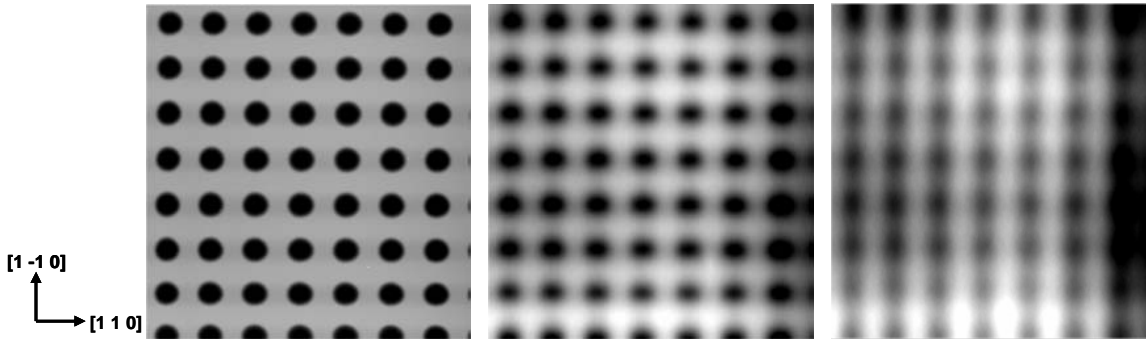
with $\lambda_x \cdot \frac{\partial^2 h}{\partial x^2} + \lambda_y \cdot \frac{\partial^2 h}{\partial y^2}$. The x axis correspond to the [1 1 0] direction and the y axis

correspond to [1 -1 0] direction respectively. The ratios $\frac{v_y}{v_x} = 5$ and $\frac{\lambda_y}{\lambda_x} = 10$

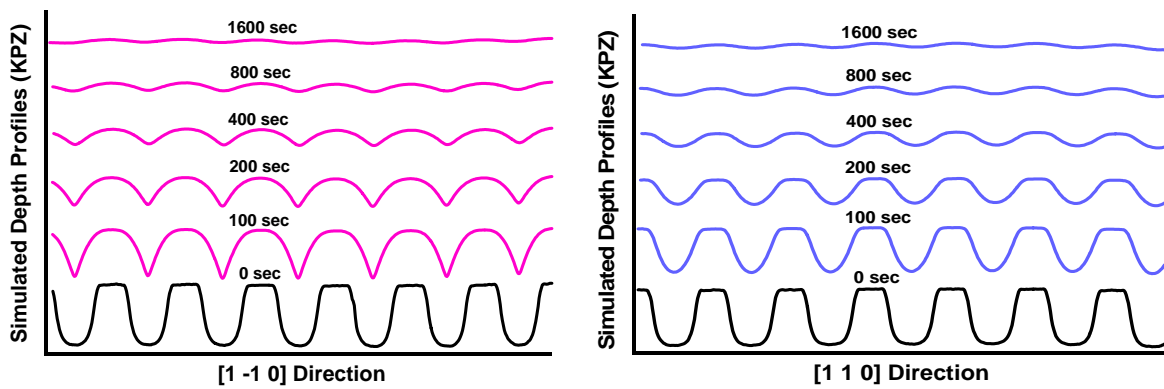
reproduces the anisotropy similar to what we see in the experiments. The relative magnitudes between the v 's and λ 's are chosen within the range such that the growth terms play a significant role in the evolution. The equations are numerically integrated with a negligible noise term. The reason being, as we will show later, the dominant features in the topography remain those at the pattern length scale over the growth range we have explored. This implies that the local fluctuations due to instantaneous and local variations in the flux are not significant for understanding our results.

Surface morphology for the KPZ model after 1600 sec of simulated growth (Fig 5-7 (a)) shows the pits are partially smeared out in the [1 -1 0] direction, similar to what we see in Fig 5-6 (a). The depth profiles shows that (Fig 5-7 (b)) that the simulated growth very quickly produces cusps at the bottom of each pit center along the [1 -1 0] fast evolution direction and the pits evolve into sinusoidal modulation along the [1 1 0] slow evolution direction, also similar to what we see in Fig 5-6 (b). However there

is no indication of an initial amplification in corrugation which is in contrast to our observations.



a) Surface Morphology of 0.7 micron diameter and 1.4 micron spacing region; initial surface, after 800 sec and after 1600 sec simulation respectively.

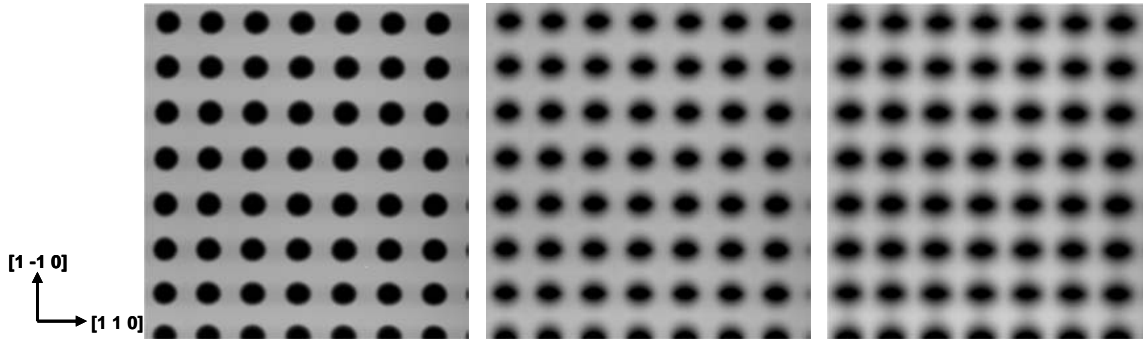


b) Simulated depth profiles along the orthogonal directions

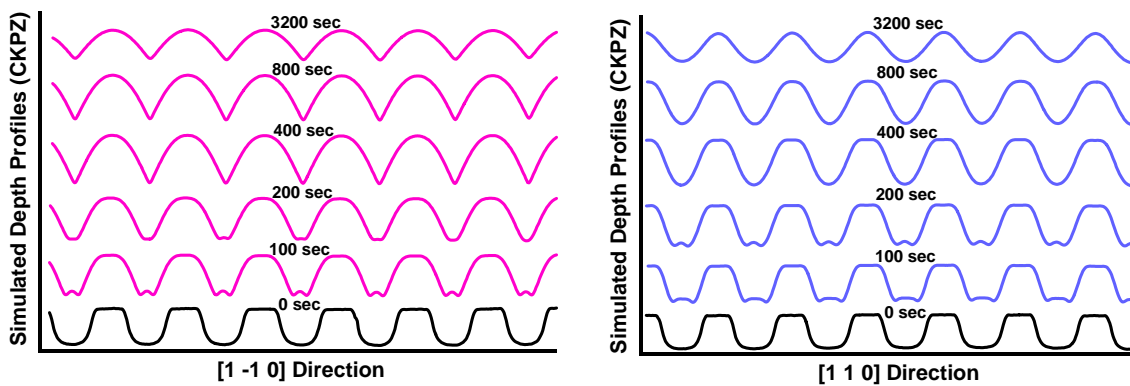
Figure 5-7: Surface Morphology and Depth profiles from simulations based on the KPZ Model.

In the CKPZ model, the most noticeable effect is the anisotropic evolution of the pits into elliptical shape, Fig 5-8 (a). The build up of material between pits is not as pronounced as in case with the KPZ model. Simulated growth depth profiles (Fig 5-8 (b)), show trench formation along the $[1 -1 0]$ direction at the bottom of the pits, whose edges coalesce to form single cusps at pit bottoms as growth proceeds. The pits evolve into sinusoidal profile along the $[1 1 0]$ direction. Significantly, in this

case we find an initial amplification of the pattern corrugation, similar to what we see in our experiments.



a) Surface Morphology of 0.7 micron diameter and 1.4 micron spacing region; initial surface, after 800 sec and after 3200 sec simulation respectively

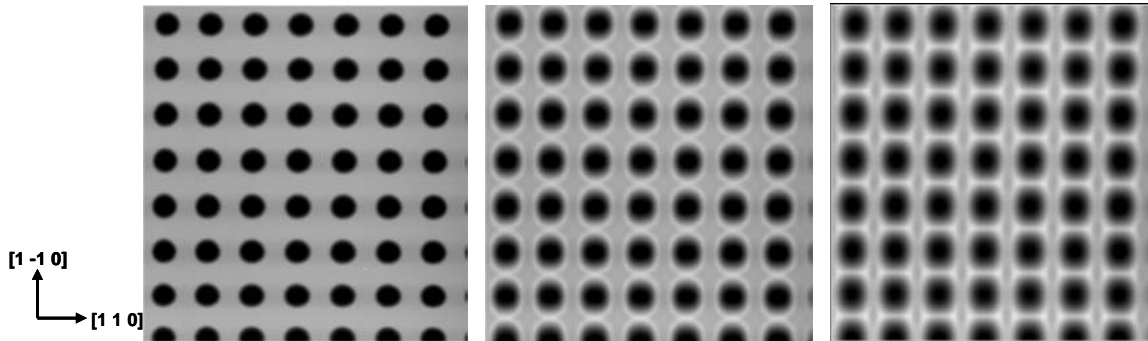


b) Simulated Depth profiles along the orthogonal directions

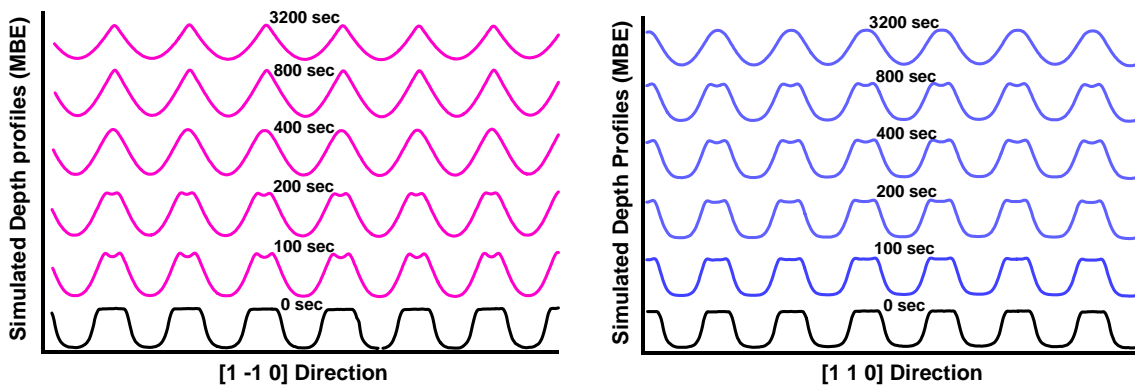
Figure 5-8: Surface Morphology and Depth profiles from simulations based on the CKPZ Model.

The surface morphology after simulated growth based on the MBE model of Lai and Das Sarma (Fig 5-9 (a)) appears quite different from the AFM image shown in Fig 5-6 (a). Initially a ring shape protrusion forms around each pit. With further simulated growth these protrusions merge forming persistent cusps in between the pits along the $[1 -1 0]$ direction, whereas the pit eventually evolves into a sinusoidal profile along

the $[1\ 1\ 0]$ direction (Fig 5-9 (b)). The evolution is quite different from what we see in our experiments; hence it allows us to exclude this model.



a) Surface Morphology of 0.7 micron diameter and 1.4 micron spacing region; initial surface, after 800 sec and after 2400 sec simulation respectively

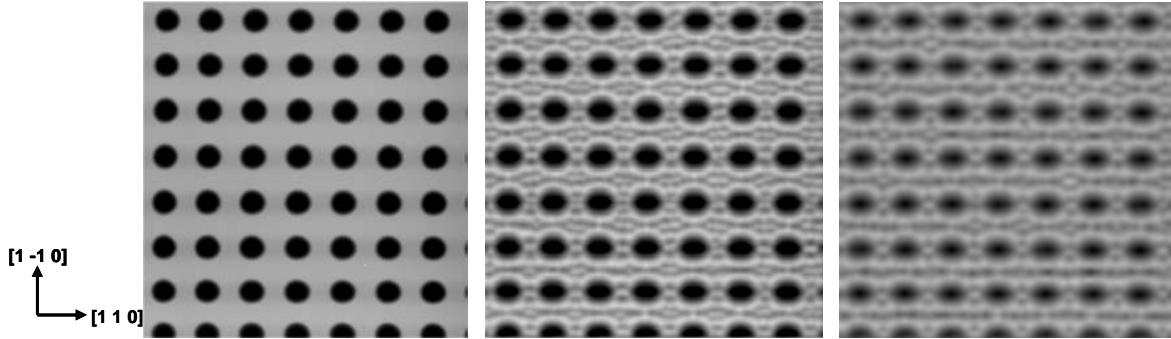


b) Simulated depth profiles along the orthogonal directions

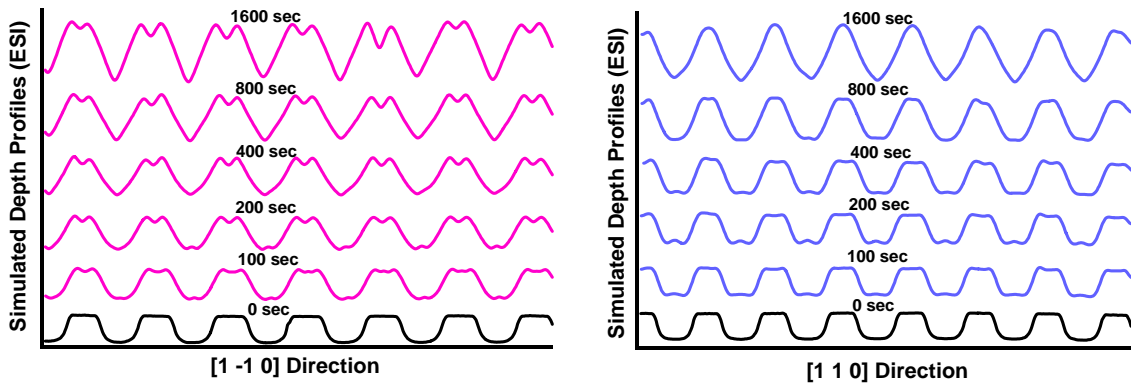
Figure 5-9: Surface Morphology and Depth profiles from simulations based on the MBE Model by LDS.

Finally, Figure 5-10 (a) shows the surface morphology after simulated growth according to the model proposed by Johnson et al. The pits evolve anisotropically but the overall evolution is quite different to what we see from our experiments. Mounds are formed which join to the sidewall of pits, forming quasi-continuous rings about them (Fig 5-10 (b)). The sidewalls of the pits are nearly linear, and the angle they

make with respect to (001), as well as the corrugation amplitude continues to grow monotonically with time. We therefore exclude this model as well.



a) Surface Morphology of 0.7 micron diameter and 1.4 micron spacing region; initial surface, after 800 sec and after 1600 sec simulation respectively



b) Simulated depth profiles along the orthogonal directions

Figure 5-10: Surface Morphology and Depth profiles from simulations based on the ESI Model.

Since only the KPZ and the CKPZ models are in qualitative agreement with our experiments we restrict a more complete analysis of the length scale dependence to these models. The results of these models are qualitatively different from each other. The KPZ equation shows a monotonic variation of corrugation amplitude with lateral length scale with monotonic decay with growth for all pit diameters (Fig 5-12). This is inconsistent with what we see in our experiments as shown in Fig 5-11.

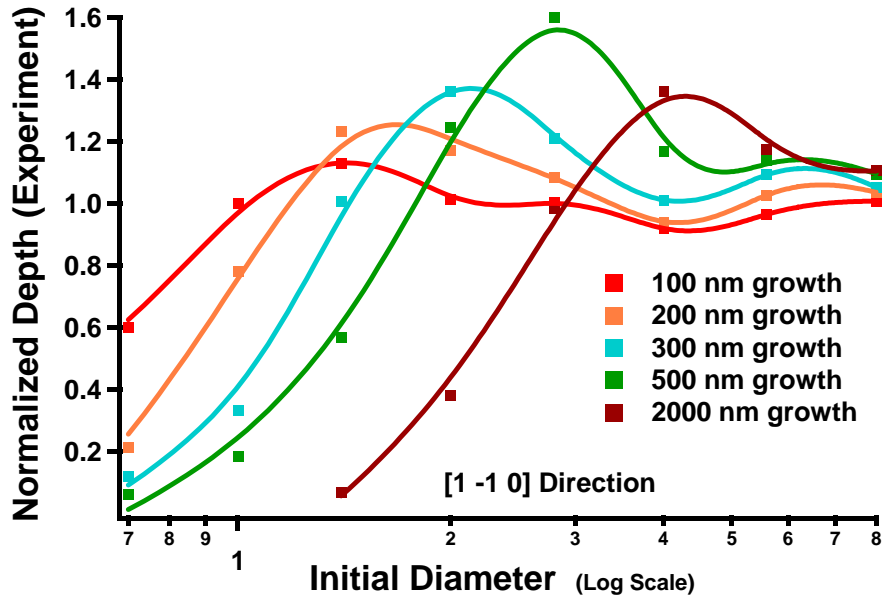


Figure 5-11: Summary plot of Normalized Depth vs. initial pit diameters after various stages of GaAs Homoepitaxial growth along the [1 -1 0] fast evolution direction on patterned GaAs (001).

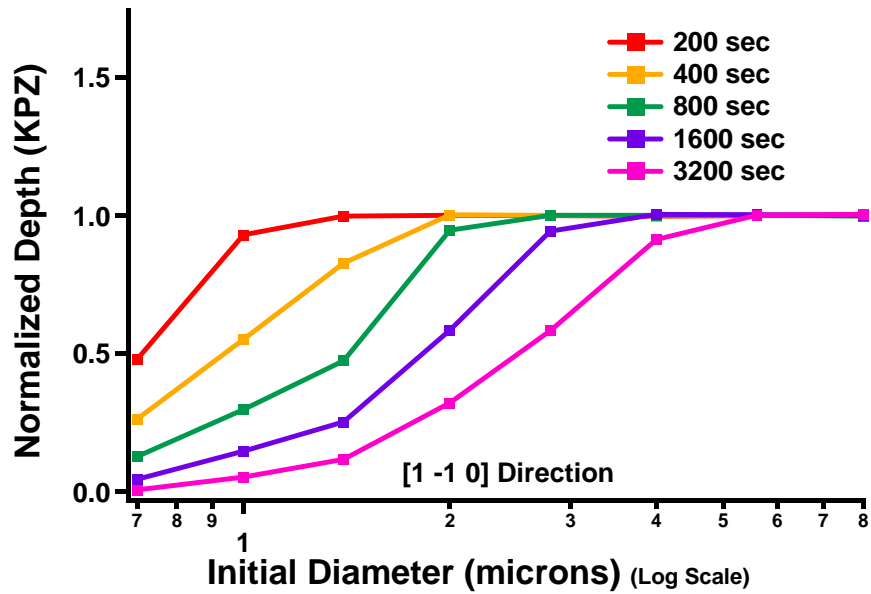


Figure 5-12: Summary plot of Normalized Depth vs. initial pit diameters for numerical simulations of the KPZ model.

The CKPZ model however shows a peak in corrugation with respect to the length scale which moves to larger length scales with further growth (Fig 5-13). The amplitude of the corrugation also behaves non-monotonically with growth with initial increase in amplitude followed by decay which is qualitatively consistent with our experimental results. Thus the CKPZ model is in closest agreement with our experimental results. However there are some differences, most notable being that the experimental results shows the peak corrugation amplitude varies with growth, while those predicted by the CKPZ model are approximately constant.

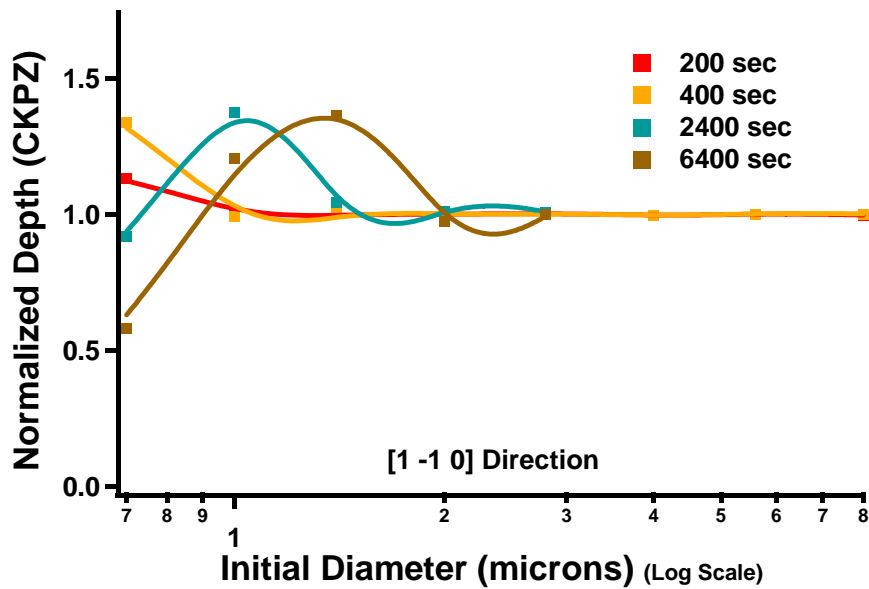


Figure 5-13: Summary plot of Normalized Depth vs. initial pit diameters for numerical simulations of the CKPZ model.

A lack of complete quantitative agreement is perhaps not surprising since the continuum models like the CKPZ were developed to describe the asymptotic behavior of the surface roughness. Only those terms which dominate during this limit were kept in the height equation. Better agreement might result if additional terms were

included, since we are in the transient regime with an artificially patterned surface with large values of $|\nabla h|$. However modification of this and other continuum models is beyond the scope of this thesis. On the other hand our simulations provide a convenient test for existing models, and also a method to study and develop new models.

Chapter 6

SUMMARY AND FUTURE WORK

To summarize, our experimental observation of the evolution of corrugation of patterned GaAs (001) for Multi-layer and Homoepitaxial MBE growth shows a non-monotonic behavior both with respect to lateral length scale and the amount of material grown at typical MBE growth conditions. There exists a characteristic peak which separates regimes of amplification and decay. This behavior is generic to MBE growth in this system. Among the four models we have compared, CKPZ model is the closest to what we see in our experiments qualitatively. An equivalent microscopic model based on the physical process is needed to judge if this agreement is merely accidental. Further experiments in which temperature is varied, presently underway promise to shed some light on a possible physical meaning of the nonlinear term in CKPZ and related models which cause the interesting behavior observed here [36].

BIBLIOGRAPHY

- [1] International Conference on Solid State Crystals 2000: Epilayers and Heterostructures in Optoelectronics and Semiconductor Technology by Jaroslaw Rutkowski , Leszek Kubiak , Jakub Wenus (SPIE-Intl Society for Optical Engineering, April, 2001)

- [2] G. Ehrich and F. J. Hudde, J. Chem. Phys. 44, 1099 (1996)

- [3] R. L. Schwoebel and E. J. Shipsey, J. Appl. Phys. 37, 3682 (1966)

- [4] M. D. Johnson, C. Orme, A.W. Hunt, D. Graff, J. Sudijono, L. M. Sander, and B. G. Orr. Stable and Unstable Growth in Molecular Beam Epitaxy. Phys. Rev. Lett. 72, 116 (1994)

- [5] G. Lengel, R. J. Phaneuf, E. D. Williams, S. Das Sarma, W. Beard and F. G. Johnson. Nonuniversality in mound formation during semiconductor growth. Phys. Rev. B 60, R8469 (1999)

- [6] Georgios Apostolopoulos, Jens Herfort, Lutz Daweritz, Klaus H. Ploog, and Martina Luysberg. Reentrant mound formation in GaAs (001) homoepitaxy observed by ex-situ Atomic Force Microscopy. Phys. Rev. Lett. 84, 3358 (2000)

- [7] A. Ballestad, B. J. Ruck, M. Adamcyk, T. Pinnington, and T. Tiedje. Evidence from the Surface Morphology for Nonlinear Growth of Epitaxial GaAs Films. Phys. Rev. Lett. 86, 2377 (2001)

- [8] Fractal Concepts in Surface Growth by A-L. Barabasi and H. E. Stanley, Cambridge University Press, (1995)
- [9] Toshio Ogino, Hiroki Hibino and Yoshikazu Homma, Patterning assisted control for ordered arrangement of atomic steps on Si (111) surfaces. Jpn. J. Appl. Phys. 34, L668 (1995)
- [10] Pierre-David Szkutnik, Dirk Sander, Frederic Dulot, Alexander Kraus, Christel Jeckstiess, Francois Arnaud d'Avitaya, Henning Neddermeyer, and Margrit Hanbucken. Scanning tunneling microscopy study of the stability of nanostructures on Si (111) at elevated temperature. Surface Science 507-510, 615 (2002)
- [11] Jack M. Blakely and So Tanaka. Atomic Step Dynamics on Periodic Semiconductor Surface Structures; S. Tanaka, C. C. Umbach, J. M. Blakely, M. Mankos, and R. M. Tromp. Fabrications of Arrays of Large Step free Regions on Si (001). Appl. Phys. Lett. 69, 1235 (1996)
- [12] H. C. Kan, S. Shah, T. Tadayyon, K. Limpaphayom and R. J. Phaneuf, Transient Evolution of Surface Roughness on Patterned GaAs (001) during Homoepitaxial Growth. Phys. Rev. Lett. 92, 146101 (2004)
- [13] Futurrex Inc., 12 Cork Hill Road, Franklin, NJ 07416, USA. Ph: 973-209-1563
- [14] Oxford Instruments GmbH, 130A Baker Avenue Extension, Concord MA 01742, USA. Tel: 001- (0)978-369-9933
- [15] Digital Instruments, Veeco Metrology Group, 112 Robin Hill Road, Santa Barbara, CA 93117. Ph: (805) 967-1400

- [16] American Xtal Technology, 4487 Technology Drive, Fremont, California 94538, USA. Tel: (510) 226-4300
- [17] M. Kardar, G. Parisi, and Y. C. Zhang, Dynamic scaling of growing interfaces. *Phys. Rev. Lett.* 56, 889-892 (1986)
- [18] T. Halpin-Healy and Y. C. Zhang, Kinetic roughening phenomena, stochastic growth, directed polymers and all that. *Aspects of multidisciplinary statistical mechanics, Physics Reports*, 254, 215-414, (1995)
- [19] Hwa T. and M. Kardar, Avalanches, hydrodynamics and discharge events in models of sand piles. *Phys. Rev. A*, 45, 7002-7021, (1992)
- [20] N. G. Van Kampen, *Stochastic Process in Chemistry and Physics*, North-Holland, Amsterdam, (1981)
- [21] T. Hwa and M. Kardar, *Phys. Rev. Lett.* 62, 1813, (1989)
- [22] S. Katz, J. L. Lebowitz and H. Spohn, *J. Stat. Phys.* 34, 497, (1984)
- [23] R. Bruinsma and G. Aeppli, *Phys. Rev. Lett.* 52, 1547, (1984)
- [24] J. Koplik and H. Levine, *Phys. Rev. B*, 32, 280, (1985)
- [25] V. P. LaBella, et al., *Phys. Rev. Lett.* 83 (15), 2989, (1999)
- [26] M. Itoh, et al., *Phys. Rev. Lett.* 81 (3), 633, (1998)
- [27] Z. W. Lai and S. D. Sarma, *Physical Review Letters*, 66 (18), 2348, (1991)

- [28] M. D. Johnson et al., *Physical Review Letters*, 72 (1), 116, (1994)
- [29] T. Sun, H. Guo and M. Grant, *Physical Review A*, 40 (11), 6763, (1989)
- [30] S. Shah, T. J. Garrett, K. Limpaphayom, T. Tadayyon-Eslami, H. C. Kan and R. J. Phaneuf, A patterning based investigation of the length-scale dependence of the evolution of interfaces during GaAs/AlAs multilayer growth, *App. Phys. Lett.* 83 (21), 4330-4332, November 24, 2003
- [31] Koranan Limpaphayom, Private Communication
- [32] Taesoon Kwon, Private Communication
- [33] Lynn Calhoun, Private Communication
- [34] Kan, Private Communication
- [35] Newman, T. J. and A. J. Bray, *J. Phys. A*, 1996, (29), 7917.
- [36] T. Tadayyon-Eslami, H. C. Kan and R. J. Phaneuf, in preparation (2004)
- [37] W.W. Mullins, *J. Appl. Phys.* 28, 333 (1957).